Single Mol. **3** (2002) 1, 49-61

Analysis of Ligand Binding by Two-Colour Fluorescence Cross-Correlation Spectroscopy

Thomas Weidemann [A)], Malte Wachsmuth [A)], Michael Tewes [C)], Karsten Rippe [B)] and Jörg Langowski [A)]

[A)] *Abteilung Biophysik der Makromoleküle*
Deutsches Krebsforschungszentrum
Im Neuenheimer Feld 280
D-69120 Heidelberg, Germany

[B)] *Abteilung Molekulare Genetik*
Deutsches Krebsforschungszentrum
Im Neuenheimer Feld 280
D-69120 Heidelberg, Germany

[C)] *Caesar Research Center*
Friedensplatz 16
D-53111 Bonn, Germany

Correspondence:
Jörg Langowski
Deutsches Krebsforschungszentrum,
Abteilung Biophysik der Makromoleküle
Im Neuenheimer Feld 280
D-69120 Heidelberg, Germany
phone ++49-6221-423390
fax ++49-6221-42523390
e-mail jl@dkfz.de

submitted 29 Jan 2002
acepted 22 Feb 2002
published 11 Mar 2002

keywords: FCS, FCCS, receptor-ligand binding, protein-DNA interactions

Abstract

Fluorescence correlation spectroscopy (FCS) is a well-established method for the analysis of freely diffusing fluorescent particles in solution. In a two-colour setup, simultaneous detection of two different dyes allows the acquisition of both the autocorrelation of the signal of each channel and the cross-correlation of the two channels (fluorescence cross-correlation spectroscopy, FCCS). The cross-correlation function is related to the amount of diffusing particles carrying both dyes and can be used for monitoring a binding reaction. Here we develop a formalism for a quantitative analysis of ligand binding from a combination of the auto- and the cross-correlation amplitudes. Technical constraints, like the focal geometry, background signal and cross-talk between the detection channels as well as photophysical and biochemical effects which modulate the brightness of the particles are included in the analysis. Based on this framework a comprehensive treatment for the determination of two-component binding equilibria by FCS/FCCS is presented.

Introduction

Fluorescence correlation spectroscopy (FCS) is a method that analyzes fluorescence fluctuations arising from single molecules diffusing in and out of a microscopic volume. The observation volume is defined by a strongly focussed excitation laser beam and a confocally arranged optical setup for detection. The fluorescence from the excitation light is separated with filters and dichroic mirrors (Fig. 1, for a detailed description of the instrumental setup see for example [1]). Although this concept has been introduced some time

 1438-5163/01/0103-0049 $17.50+.50/0

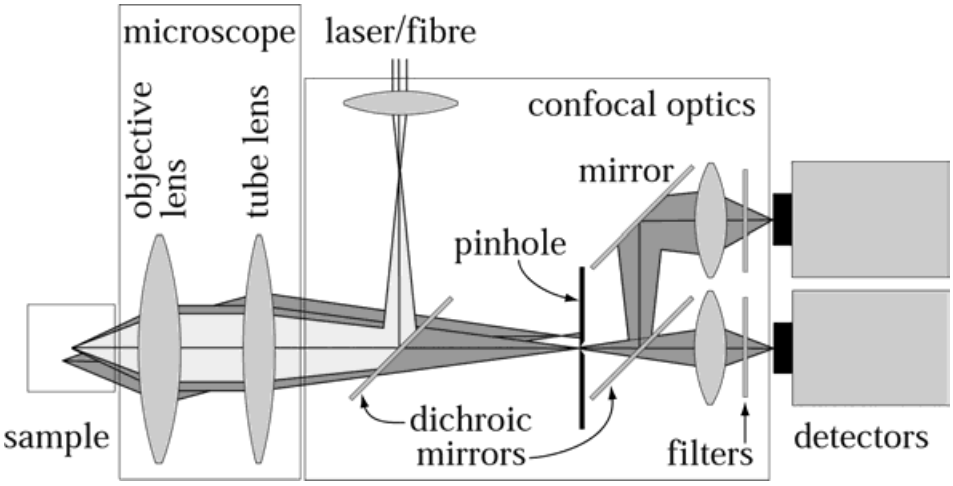

Fig. 1 *Schematic view of a confocal two-colour FCCS setup.*

ago [2,3,4], it has led to a wider range of applications only recently because of two technical improvements: the use of high numerical aperture microscope optics provides a diffraction limited illumination volume of less than a femtoliter [5]. In addition, the development of avalanche photodiodes offers a nearly tenfold increase in quantum yield compared to common photomultiplier tubes [6], so that single molecules can be detected [7]. In solution, and if no other effects on emission are present, the detected signal arises from fluctuations in the number of fluorescently labelled particles in the observation volume due to their Brownian motion. An autocorrelation analysis of the fluorescence signal yields the characteristic dwell time τ of the particles in the volume, corresponding to the decay time of the correlation function, and their concentration, reflected by the fluctuation amplitude.

An important extension of FCS is the simultaneous detection of the two colour-channels [8, 9, 10, 11, 12, 13, 14] with basically the same instrumentation principle. However, two spectrally distinct dyes are excited, usually at two different wavelengths. Their emitted fluorescence is split subsequently by dichroic mirrors and filters into the respective detection channels. With two-colour FCS, a cross-correlation analysis can be made (FCCS), where the signals of the two channels are time correlated with each other to collect information only about particles that carry both types of dyes. In order to extract parameters like diffusion coefficients, relative quantum yields, and relative concentrations of components distinct in their hydrodynamic properties, an analytical correlation function is fitted to the experimental data. The model functions were derived for translational diffusion with one-colour FCS in several geometric realizations of excitation and detection [5, 15, 16, 17] and can only be applied to two-colour FCS under idealized conditions [12]. Effects like cross-talk between the detection channels or chromatic aberrations, i.e. incomplete overlap of the detection volumes can lead to significant deviations from the one-colour model functions.

Interactions between small ligands and macromolecules as well as multimerization of molecules are of general interest in biochemistry. They are described at equilibrium by the dissociation constant K_d for a given complex which is related to its free energy of formation ΔG as $K_d = e^{\Delta G / RT}$. To determine these quantities free in solution under true equilibrium conditions a number of methods have been applied such as absorbance, fluorescence intensity, fluorescence depolarisation, or circular dichroism. The prerequisite here is that the signal used for the titration changes upon binding. This is sometimes hard to achieve, and even if it is fulfilled, these techniques often require relatively large amounts of substance. In addition, dissociation constants smaller than 10^{-8} M are difficult to access because very often the signal is not sensitive enough. In this respect FCS/FCCS is a promising method, since it is capable of determining concentrations and therefore dissociation constants down to the picomolar range. For many physiological systems, for example the binding of proteins to DNA, dissociation constants are in this range.

How are binding parameters linked to observables in FCS? The main effects on the signal are changes in diffusion behaviour and altered fluorescence properties, both being related to biologically relevant processes like binding and enzymatic or chemical reactions (for review see [18, 19]). Altered fluorescence properties can be time-dependent, such as triplet transitions, photobleaching, or flickering. These effects cause modulations of the intensity signal and have been the subject of theoretical and experimental investigations [20, 21, 22]. Time-independent fluorescence changes at equilibrium can occur when ensembles of particles show a different brightness due to quenching effects or variations in the number of fluorophores. These time-independent alterations have been investigated with FCS, e.g. by Thompson and coworkers who studied clustering of fluorescent lipids and receptors at the cell surface [23, 24, 25, 26] by analysis of higher order correlations. More recently, molecular brightness distributions have been addressed with a method called photon counting histogram (PCH) or

fluorescence intensity distribution analysis (FIDA) based on an amplitude analysis of fluorescence fluctuations [27, 28].

In the last few years, the improvement of the FCS technology has led to several applications in which the appearance of a component with a longer diffusion time was used to monitor binding. Equilibrium constants for simple receptor-ligand binding including protein-DNA interactions have been measured [29, 30, 31, 32, 33]. However, this approach is limited to systems where the difference in diffusion times between ligand and complex are relatively large. Alternatively, the cross-correlation signal can be used to monitor binding as described by Schwille et al. [14], who followed association kinetics of single DNA strands into a DNA duplex. Rigler and coworkers used FCCS to detect the hybridization of DNA primers and to evaluate polymerase chain reactions [13, 34], and Kettling et al. monitored the kinetics of endonuclease activity by FCCS [9]. In a recent study, the simultaneous binding of two DNA ligands labelled with different fluorophores to an unlabelled protein complex was analyzed by FCCS/FCS, and ΔG values for the formation of different species were extracted from the data [35]. Here we present a general formalism for quantitative two-colour FSC as introduced previously [36] and derive a theoretical analysis for the determination of binding parameters from a combination of auto- and cross-correlation functions.

Theory and Discussion

1. Laser – Fluorophore – Detector

The light intensity measured in a fluorescence experiment is a result of photon absorption, electronic excitation, and radiative decay of fluorescent molecules in the solution and detection of their emitted photons. Each part of the process is influenced by quantities specific for the technical setup and the fluorescent probes. For clarity these quantities are divided into spatial and spectral dependencies: the illumination profile is given by the product of the laser power P_i and the point spread function of the microscope optics, $PSF_i(\vec{r})$. Both the beam profile of the incident laser light at the back aperture of the optical system and the transformation of this profile by the optical system define $PSF_i(\vec{r})$. Working with discrete laser lines allows simple indexing (i=1, 2) with no need to integrate over the wavelength. The fluorophores are characterized by their extinction coefficients $\varepsilon(\lambda_{ex,i})$ and their emission spectra $q(\lambda_{ex,i})$, which can be regarded as the relative probability for emitting a photon with wavelength λ_{em}.

Depending on its emission position $\vec{r}$ in the sample volume, a photon is detected with a certain probability in channel j, which is referred to as the *geometrical transmission function* $GTF_j(\vec{r})$. By the *spectral transmission function* $STF_j(\lambda_{em})$ all spectral properties of filters, detectors, etc. are taken into account. The photon flux at the detector j=1, 2 produced by a single fluorophore at the position $\vec{r}$ is therefore given by

$$f_j(\vec{r}) = \underbrace{P_i \cdot PSF_i(\vec{r}) \cdot \varepsilon(\lambda_{ex,i})}_{\text{excitation}} \cdot \underbrace{GTF_j(\vec{r}) \cdot q_j(\lambda_{em}) \cdot STF_j(\lambda_{em}) d\lambda_{em}}_{\text{emission +detection}} \tag{1}$$

assuming linear behaviour of all components (which is usually the case when working with intensities in the range of several kW cm^{-2}). For simplification we introduce the *colour matrix* $\sigma_{ij} = e(\lambda_{ex,i})\, q_i(\lambda_{em})\, STF_j(\lambda_{em}) d\lambda_{em}$. The remaining spatial function defines the observation volume according to $\psi_{ij}(\vec{r}) = PSF_i(\vec{r}) \cdot GTF_j(\vec{r})$ and is therefore termed the *detection function*. If the sample is exposed to more than one laser line, as in cross-correlation measurements, or if the diffusing molecules carry more than one (n_t=1, 2...) or different types of fluorophores (t=*a, b,...*) we have to sum over the individual excitation lines and *colour matrices*

$$f_j(\vec{r}) = \sum_i P_i \Big(\sum_t n_t \sigma_{ij}^{(t)} \Big) \Psi_{ij}(\vec{r}). \tag{2}$$

2. Correlation of One Species

Now we assume a model system of N identical, non-interacting, freely diffusing fluorescent particles in a sample volume V. During the experiment a digital correlator computes the normalized correlation function of the fluorescence intensity $F_j(t)$ at the detector j:

$$G_{kl}(\vec{r}) = \frac{\langle F_k(0) F_l(\tau) \rangle}{\langle F_k \rangle \langle F_l \rangle} - 1 = \frac{\langle \delta F_k(0) \delta F_l(\tau) \rangle}{\langle F_k \rangle \langle F_l \rangle}. \tag{3}$$

$G_{kl}(\vec{r})$ carries two indices allowing simultaneous treatment of auto- (k=l↔j) and cross-correlation ($k \neq l \leftrightarrow \times$). Deviations from the mean value are represented by δ. The parameter τ is the lag time and the brackets indicate averaging over time. $F_j(t)$ is always the sum of the contributions of all fluorescent particles in the sample, depending on their position with respect to the laser focus, $F_j(t) = \sum_{n=1}^{N} f_j(\vec{r}_n(t))$. It is proportional to the number N_{ob} of particles in the observation volume. Then Eq. (3) transforms into

$$G_{kl}(\tau) = \frac{\sum_n \langle \delta f_k(\vec{r}_n(0)) \delta f_l(\vec{r}_n(\tau)) \rangle}{\sum_n \langle f_k \rangle \sum_n \langle f_l \rangle} = \frac{N \langle \delta f_k(\vec{r}(0)) \delta f_l(\vec{r}(\tau)) \rangle}{N \langle f_k \rangle N \langle f_l \rangle} = \frac{1}{N} g_{kl}(\tau), \tag{4}$$

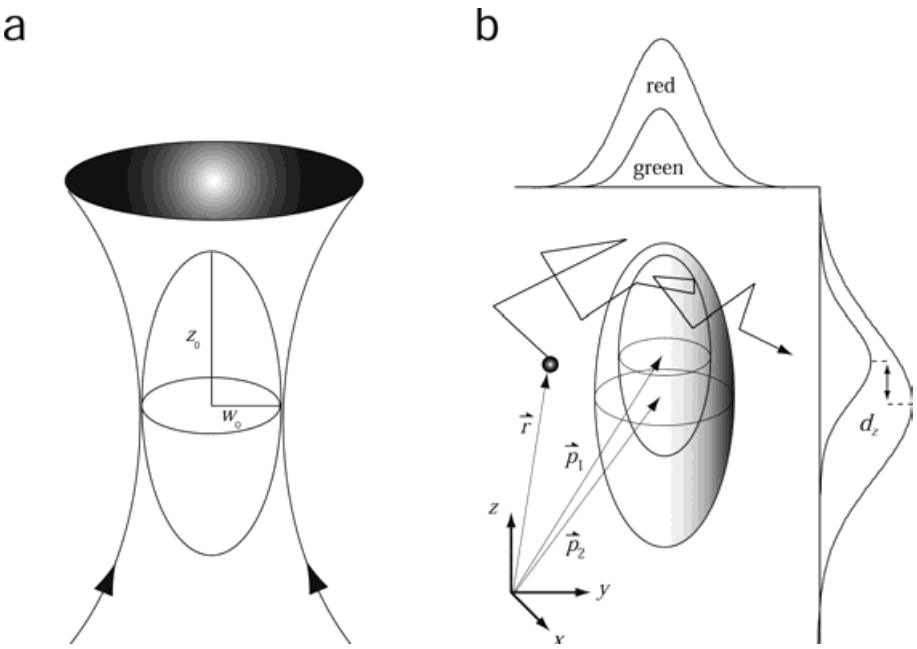

Fig. 2. *Focal geometry.* ***(a)*** *In a confocal setup with high numerical aperture, the detection probability can be described by rotational Gaussian functions with 1/e² -radii w_0 transversal and z_0 parallel to the optical axis z.* ***(b)*** *The foci of a two-colour setup centred at positions $\vec{p}_1$ for the green and $\vec{p}_2$ for the red excitation wavelength differ in size and can show chromatic shifts, here exemplary drawn parallel to the optical axis, d_z .*

and $G_{kl}(\tau)$ can be reduced to the correlation function of a single molecule $g_{kl}(\tau)$. Eq. (3) and (4) imply two important properties of FCS: First, assuming Poissonian statistics for number fluctuations of a single species, with $\langle \delta N^2 \rangle = \langle N \rangle$, the amplitude is the inverse average number of particles in the observation volume $G_{kl}(0) = 1/\langle N_{ob} \rangle$. Second, the total correlation curve is the sum of the single particle correlation curves, which is important for the analytical treatment of spectral classes as described below.

3. Correlation Functions in a Two-Colour Setup

In order to extract diffusion coefficients and concentrations an analytical expression for the correlation function is fitted to the data. The correlation functions for translational diffusion and chemical reactions are based on the assumption that the $\Psi_{ij}(\vec{r})$ are two- or three-dimensional Gaussian functions. It turns out that this approximation is justified for low numerical aperture systems [37] as well as for several diffraction limited setups [5,6]. In a two-colour setup, additional aspects have to be considered. First, the size of the observation volumes is wavelength dependent. The linear dimensions are in first order proportional to the excitation wavelength, resulting in focal volumes differing by a factor of 1.58 for the commonly used laser lines of 488 nm and 568 nm. Second, the centres of the respective foci may show an axial or lateral displacement (Fig. 2a), due to chromatic aberrations along the optical path. In confocal laser scanning microscopy, values between 50 and 100 nm have been reported [38,39], which is of the order of the beam waist and thus not negligible.

Subsequent treatment of the geometry leads to a modified correlation function (Appendix A):

$$G_{kl}(\tau) = \frac{1}{cV_{eff,\,kl}} \left(1 + \frac{4D\tau}{w_{0,eff}^2}\right)^{-1} \left(1 + \frac{4D\tau}{z_{0,eff}^2}\right)^{-\frac{1}{2}} \exp\left(-\frac{d_x^2 + d_y^2}{4D\tau + w_{0,eff}^2} - \frac{d_z^2}{4D\tau + z_{0,eff}^2}\right) \quad (5)$$

where $\vec{d} = \vec{p}_k - \vec{p}_l$ is the displacement vector between the centres of the two foci of the individual laser lines $(\vec{p}_k, \vec{p}_l)$, and $w_{0,eff}^2 = (w_{0k}^2 + w_{0l}^2)/2$ and $z_{0,eff}^2 = (z_{0k}^2 + z_{0l}^2)/2$ define the *1/e²* radii of the gaussian profiles, perpendicular and parallel to the optical axis (Fig. 2b), respectively. $V_{eff,kl} = \pi^{\frac{3}{2}} w_{0k} w_{0l} (z_{0k} z_{0l})^{\frac{1}{2}}$ is - apart from a factor of about 1.4 - the volume of a rotational ellipsoid which is usually defined as the observation volume (Fig. 2a). For autocorrelation ($\vec{d} = 0$), the exponential term vanishes and the function reduces to the well known form. But for a cross-correlation, a displacement produces a noticeable reduction of the amplitude and a slightly slower decay of the correlation function, corresponding to an apparently longer diffusion time (Fig. 3).

In experimental practice, additional fluorescence fluctuations can also result from intramolecular processes like intersystem crossing between singlet and triplet states in dyes or protonation of the chromophore in autofluorescent proteins. They lead to additive exponential decays in the autocorrelation functions for short correlation times [20,21], but do not appear in the cross-correlation. In this paper, all correlation functions and amplitudes used are already corrected for this, i.e., they are purely diffusion-induced.

$$\alpha A + \beta B \underset{k_2}{\overset{k_1}{\rightleftharpoons}} A_\alpha B_\beta \qquad (6)$$

4. Correlation of Multiple Species

Particles can differ in their hydrodynamic behaviour and in their molecular brightness. The one-species correlation function is based on the assumption that the system is at thermodynamic equilibrium and the particles do not interact. The latter does not hold true when looking at chemical reactions or binding in solution. A reversible association reaction,

implies an additional constraint: the mean lifetime of the complex should be significantly longer than its diffusion time, $1/k_2 >> \tau_{diff}$. Then, a dissociation during the residence in the focal volume is very unlikely and the same is true for complex formation. In other cases the analysis of the correlation functions becomes less feasible [40]. In analogy to the additive contribution of single fluorophores to Eq. (4), the correlation function can be written as the sum over single species (s=1, 2, ...) weighted with the product of their mean intensities

$$G_{kl}(\tau) = \frac{\sum_s c^{(s)} \tilde{F}_k^{(s)} \tilde{F}_l^{(s)} \tilde{G}_{kl}^{(s)}(\tau)}{\sum_s c^{(s)} \tilde{F}_k^{(s)} \sum_s c^{(s)} \tilde{F}_l^{(s)}} = G_{kl}(0) V_{eff,kl} \sum_s \rho^{(s)} \tilde{G}_{kl}^{(s)}(\tau) \qquad (7)$$

To indicate the concentration dependence, we have introduced the *characteristic intensities* $\tilde{F}_j^{(s)} = \left\langle F_j^{(s)} \right\rangle / c^{(s)}$ and the *characteristic one species correlation functions* $G_{kl}^{(s)}(\tau) = c^{(s)} G_{kl}^{(s)}(\tau)$ which represent the respective properties of a 1 M = 1 mol/l solution of each species.

As $\tilde{G}_{kl}^{(s)}(\tau)$, $\tilde{F}_k^{(s)}$ and $\tilde{F}_l^{(s)}$ are directly accessible by measuring purified samples, a system of up to three spectral species (even with the same diffusion behaviour) can be described by recording two auto- and one cross-correlation functions. This increases the "resolution" of a given system because with the typical signal-to-noise ratios of an FCS experiment, only up to three species can be distinguished in terms of hydrodynamical properties when fitting the second part of Eq. (7) to FCS data [41]. The obtained ratios $\rho^{(s)}$ directly reflect the concentrations of the subspecies according to $c^{(s)} = \rho^{(s)} c$ when the components show similar brightness, otherwise one has to account for some deviations (see next section). With one-colour FCS, an increase of the diffusion time or an increase of the amplitudes has been exploited to study the binding of small fluorescent molecules to a polymer or the multimerization of a particle. There are two difficulties with this approach: the diffusion time depends only weakly on molecular mass ($\tau_{diff} \propto M^{1/3}$ for globular proteins) and the resolution is quite low. Second, although the behaviour of the amplitude is linear, the one-colour FCS signal reflects not only the average number of particles but also photobleaching, quenching in the bound state, or photophysical transitions into dark states of the fluorophore. In a cross-correlation experiment, however, ligands and receptors are labelled in different colours and the amplitude will increase exclusively with the number of complexes carrying both types of dyes.

5. Influence of Quenching-Related Effects

The quantum yield of the fluorophore is often changed in the bound state due to altered local chemical environments. Although labelling protocols are often followed by extensive purification steps, removing unbound dye to less than picomolar concentrations can be a hard task. Moreover, quenching can occur through molecular rearrangement of the labelled molecules. In all cases, one encounters a mixture of at least two species differing in an arbitrary but defined magnitude of brightness.

Eq. (7) implies that the amplitude of the correlation function of a mixed solution does no longer reflect the total number of particles N_{ob} in the observation volume, since the particles contribute weighted with the square of their *characteristic intensities*. If we relate their weights according to $F_j^{(s)} = \eta_j^{(s)} F_j^{(0)}$, the amplitude is always changed compared to a standard solution with the same total concentration of fluorophore [18, 42]:

$$G_{kl}(0) = \frac{1}{c V_{eff}} \frac{\sum_s \eta_k^{(s)} \eta_l^{(s)} c^{(s)}}{\sum_s \eta_k^{(s)} c^{(s)} \sum_s \eta_k^{(s)} c^{(s)}}. \qquad (8)$$

Since an increased quantum yield of one species is equivalent to quenching of the other species, either of these two effects will affect the correlation function in the same way, namely increase $G_{kl}(0)$. Quenching of less than 30% ($\eta > 0.7$) of a component does not increase the amplitude more than 5%, independent of the molar ratio of quenched dye. However, stronger quenching effects are frequently encountered in binding assays, as well as a strong increase of the quantum yield in the case of association (see next section).

If the components can be distinguished on the basis of their diffusion times, the respective fractions $\rho^{(s)}$, obtained from fitting Eq. (5) with Eq. (7) to the experimental data, are biased in favour of the brighter components. This can be adjusted by normalizing with the quantum yields, then

$$\rho_{cor}^{(s)} = \frac{c^{(s)}}{\sum_s c^{(s)}} = \frac{\rho^{(s)} / \eta_k^{(s)} \eta_l^{(s)}}{\sum_s \rho^{(s)} / \eta_k^{(s)} \eta_l^{(s)}} \qquad (9)$$

are the real molar ratios, indexed with 'cor' for corrected.

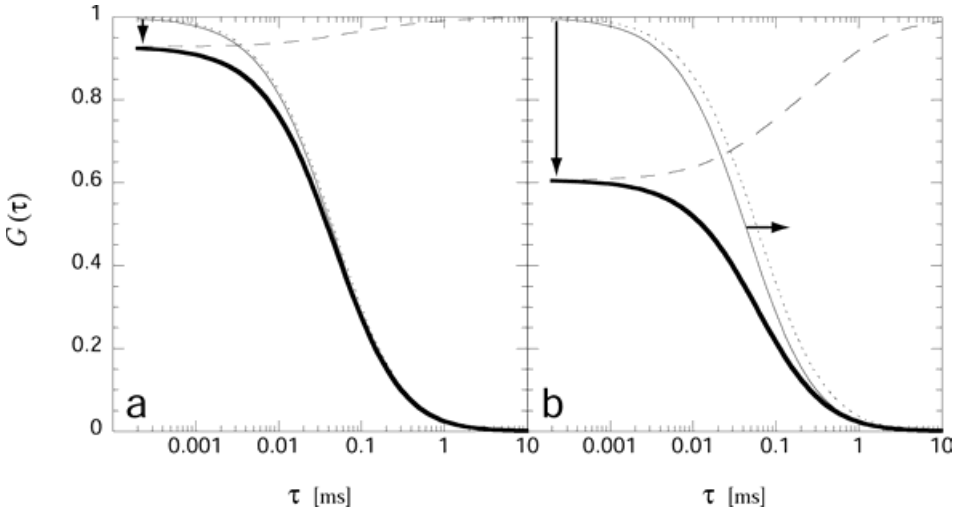

Fig. 3. *Cross-correlation functions in a two-colour setup. A typical correlation curve (thin) corresponding to a ~10 nM solution of two-coloured standard was computed for w_0 = 220 nm and z_0 = 660 nm. Chromatic displacement of $|d_{yx}| = 50$ nm, $|d_z| = 100$nm (**a**) or $|d_{yx}| = 100$ nm, $|d_z| = 330$ nm (**b**) leads to a time-dependent correction factor (broken line). The amplitude of the biased cross-correlation function (fat) appears reduced (vertical arrows) and the function is also shown normalized (dotted), in order to visualize an increase of an apparent correlation time (horizontal arrow) which would be obtained by fitting with Eq. (5) without displacement.*

6. Association and Multiple Binding Sites

Each monomer of a binding reaction can carry a defined number of fluorophores. However, the number of labelling sites is often not known. Proteins tagged with reactive derivatives of synthetic fluorophores usually expose several accessible functional groups. In addition, the number of labelling sites may vary due to *in vivo* modifications of the isolated protein. Labelling more than one of several sites with equal affinity will give a binomial distribution of similarly diffusing particles with different but discrete numbers of bound fluorophores. Fig. 4 illustrates that the same formalism can also be applied to cases where single-labelled monomers aggregate to form oligomers: presuming that the association is not influenced by the labeling, complete oligomerization of a mixture of labelled and unlabelled monomers leads to a binomial distribution of fluorophores bound in complexes with similar diffusion behaviour. Finally, application of two dyes leads to a trinomial distribution of fluorophores (monomers) on the labelled substrate (oligomers).

For an ensemble of molecules (complexes) with n potential binding sites (degree of multimerization n), the probability for finding one with n_g bound fluorophores of type g (green) and n_r fluorophores of type r (red) is given by

$$P(n_g,n_r) = \binom{n}{n_g}\binom{n-n_g}{n_r} p_g^{n_g} p_g^{n_r} (1-p_g-p_r)^{n-n_g-n_r} \qquad (10)$$

p_g and p_r stand for the probability that one binding site in the complex carries the respective type of fluorophore (for the initial molar ratio of the monomer with the respective label) and 1-p_g-p_r , that the site remains empty (that a monomer is not labelled).

In order to calculate the correlation function by means of Eq. (7), spectral subspecies are defined by a unique combination of n_g and n_r and their concentrations are expressed by the probability to find such a composition of fluorophores, scaled with the total concentration c of labelled substrate (formed complexes): $c^{(s)}=P(n_g,n_r)c$. The *characteristic intensities* are simply the sum over single contributions of bound fluorophores $\tilde{F}_j^{(s)} = n_g\tilde{F}_j^{(g)} + n_r\tilde{F}_j^{(r)}$. Using relations for the first and second order moments of $P^{(s)}(n_g,n_r)$ (see Appendix B), we obtain for the correlation function

$$G_{kl}(\tau) = 1 - \frac{1}{n} + \frac{\left(p_g\tilde{F}_k^{(g)}\tilde{F}_l^{(g)} + p_r\tilde{F}_k^{(r)}\tilde{F}_l^{(r)}\right)}{n\left(p_g\tilde{F}_k^{(g)} + p_r\tilde{F}_k^{(r)}\right)\left(p_g\tilde{F}_l^{(g)} + p_r\tilde{F}_l^{(r)}\right)} = \frac{1}{c}G_{kl}(\tau) \qquad (11)$$

Eq. (11) becomes more transparent in the case of an idealized system with properly separated detection channels: $\tilde{F}_l^{(g)}$ and $\tilde{F}_k^{(r)}$ become zero and we get for the cross-correlation amplitude

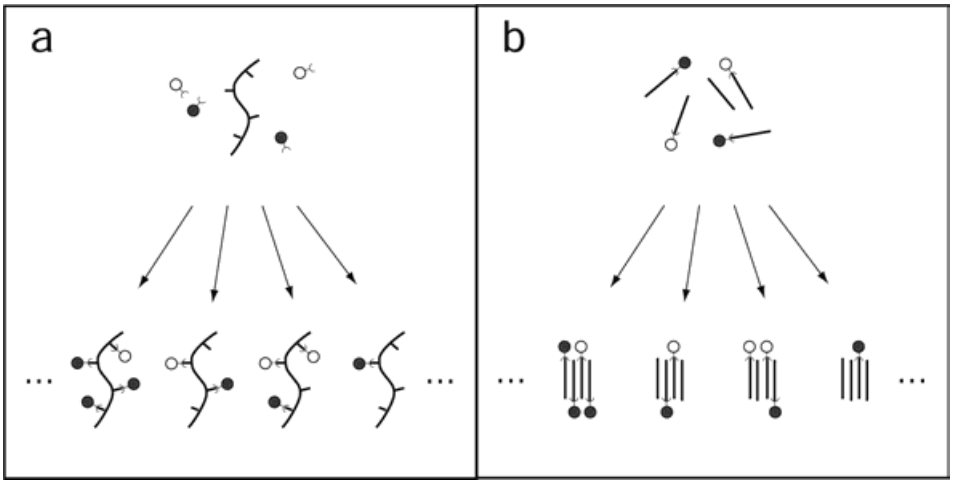

Fig. 4 *Distribution of fluorophores.* ***(a)*** *Multiple labelling of a macromolecule with small fluorescent dyes or* ***(b)*** *aggregation of uniformly labelled monomers leads to classes of similarly diffusing particles which carry distributed numbers of fluorophores.*

$$G_x(0) = \left(1 - \frac{1}{n}\right) \frac{1}{cV_{eff}} \tag{12}$$

The maximum amplitude for such an ensemble is reduced, and it is surprising that this behaviour does not depend on the labelling probabilities p_g and p_r. For better understanding we discuss a simple dimerization of monomer labelled either red or green. In the case of symmetrical fluorophore composition ($p_g = p_r$), half of the forming dimers will carry both colours, a quarter will be double-red and the remaining quarter double-green labelled, and the cross-correlation amplitude is reduced to 1/2. If one of the dyes is present in excess over the other, more single-coloured particles will be formed by the abundant dye, but at the same time more of the other dye is present in two-coloured complexes. The calculation shows that these antagonistic effects compensate each other quantitatively (of course, this argument is only valid if the signal-to-noise ratio is high enough in both channels). With an increasing number of binding sites n, the value of the cross-correlation amplitude approaches that of a homogeneously two-coloured dimer, since the probability to find single-coloured particles becomes zero.

In contrast, the autocorrelation amplitudes are increased compared to a uniformly labelled standard by an additional term $1/np_t$ which depends on the probability to find a binding site occupied with a fluorophore of a certain type t

$$G_j(0) = \left(1 - \frac{1}{n} + \frac{1}{np_t}\right) \frac{1}{cV_{eff,j}}. \tag{13}$$

The formula reflects the fact that with a lower probability p_t, less particles show fluorescence and subsequently the amplitude is increased. Note that with this kind of treatment, the distributed brightness of the formed complexes is already covered.

7. Background Correction

Although FCS in a confocal setup provides high signal-to-noise ratios, the background $U(t)$ due to noise of photon counting devices and imperfectly suppressed scattered excitation light adds non-correlated intensity to the total signal $F_{j,tot}(t) = F_j(t) + U(t)$ with $F_j(t) = \sum_s F_j^{(s)}(t)$. Inserting this into Eq. (7) results in a smaller amplitude of the correlation function and therefore in an overestimation of the concentrations observed. To account for this, a correction factor must be considered [43]

$$G_{kl}(0) = \left(1 + \frac{\langle U_k \rangle}{\langle F_k \rangle}\right)^{-1} \left(1 + \frac{\langle U_l \rangle}{\langle F_l \rangle}\right)^{-1} \frac{1}{\langle N_{ob} \rangle}, \tag{14}$$

In one-colour mode, the amplitude is reduced by less than 10% for a background below 5% in each channel. For cross-correlations, the imperfect overlap of the observation volumes results in additional non-correlating intensity, since particles may be detected in only one channel outside the two-colour observation volume. In first order approximation this contribution corresponds to the difference in observation volume between the two channels. Assuming these to depend on the illumination wavelength as $V_{eff} \propto \lambda_{ex}^3$, a cross-correlation yields merely $73\% = (568^3 - 488^3) / 568^3$ of the maximum amplitude as measured in an autocorrelation experiment. This effect may be even stronger in the case of chromatic displacement of the focal volumes.

8. General Implications of Two-Colour Excitation and Detection

Measuring simultaneously in two excitation and detection channels leads to an additional, setup-specific background due to cross-talk which is now correlated. In the framework of our description, imperfect matching of spectral characteristics between fluorophore and instrument leads to contributions of non-diagonal elements of the *colour matrix*. This includes excitation by both laser lines and emission into both detectors. We first consider implications for a single dye. In order to address this influence quantitatively we use a special case of Eq. (2) with $n_t=1$

$$\widetilde{F}_j = \sum_i P_i \sigma_{ij} \int_V \Psi_{ij}(\vec{r}) d^3 r = \sum_i \widetilde{F}_{j,i} \qquad (15)$$

$\widetilde{F}_{j,i}$ is the *characteristic intensity* at the detector *j* excited with a single wavelength $\lambda_{ex,i}$. Because of the statistical independence of the excitation processes we are allowed to apply Eq. (7), yielding an expanded expression for the *characteristic one species correlation function* $\widetilde{G}_{kl}(\tau) = cG_{kl}(\tau)$ of a single dye measured in a two-colour setup:

$$\widetilde{G}_{kl}(\tau) = \frac{\sum_{i,i'} \widetilde{F}_{k,i} \widetilde{F}_{l,i'} \widetilde{G}_{kl,ii'}(\tau)}{\widetilde{F}_k \widetilde{F}_l} \qquad ((16)$$

$\widetilde{G}_{kl}(\tau)$ appears as a sum of four apparent subspecies as a result of all modes of excitation (*ii'* = 11, 12, 21, 22) weighted with their detection probability. The observation volume of the two colour setup $V_{eff,kl} = 1 / \widetilde{G}_{kl}(0)$ is therefore already an averaged value and can differ from single-colour measurements. This difference is far from being resolvable in terms of diffusion times, but could affect the amplitudes. Note that the deviation is a result of the two colour excitation as well as the absorption properties of the fluorophore described in the *colour matrix*. This suggests to perform concentration calibrations always with the same type of dye.

In cross-correlation measurements, single diffusing fluorophores can produce a noticeable correlation due to cross-talk. If the signal-to-noise ratio is sufficiently high, the measured cross-correlation amplitude of a single dye is similar to that of a 100% two-coloured species. However, a typical approach for binding studies is to prepare two distinctly coloured populations of interacting molecules (e.g. green and red) and to start the reaction by merging the solutions. Even if both dyes show detectable cross-talk when measured separately, the characteristic intensities spilling into the "other" channel are usually low. For this reason, the initial cross-correlation amplitude of the mixture is significantly decreased. Now, successive binding of red and green particles will increase the fraction of cross correlating intensity contributing to the numerator in Eq. (7) while the denominator stays constant for a given content of labelled monomers.

9. The Ratio of Cross- and Autocorrelation Amplitude as a Measure for Binding Equilibria

We have shown that the cross-correlation amplitude depends on the concentrations as well as on the quantum yields of the particles in each channel. In order to assess dissociation constants, equilibria have to be titrated over a range of concentrations and the degree of binding has to be determined. How can the binding equilibria be measured independent from the total concentration of particles? We introduce the ratio of cross- and autocorrelation amplitude $RatioG_j$ as appropriate observable for monitoring complex formation. Eq. (7) yields:

$$RatioG_j = \frac{G_x(0)}{G_j(0)} = \frac{\sum_s c^{(s)} \widetilde{F}_k^{(s)} \widetilde{F}_l^{(s)} \widetilde{G}_x^{(s)}(0)}{\sum_s c^{(s)} \widetilde{F}_j^{(s)2} \widetilde{G}_j^{(s)}(0)} \frac{\left(\sum_s c^{(s)} F_j^{(s)}\right)^2}{\left(\sum_s c^{(s)} F_k^{(s)}\right)\left(\sum_s c^{(s)} F_l^{(s)}\right)} \qquad (17)$$

In a good approximation, the *characteristic one species correlation amplitudes* are the same for two-coloured particles in cross-correlation as for one- and two-coloured particles in autocorrelation mode, $\widetilde{G}_{kl}^{(s)}(0) \approx \widetilde{G}_{kl}(0)$. Since they represent the inverse observation volume $\widetilde{G}_{kl}(0) = 1 / V_{eff,kl}$, a factor $V_{eff,j} / V_{eff,x}$ can be extracted that is determined by geometric properties of the optical alignment as discussed in section 3. The remainder of Eq. (17) is governed by contributions of each spectral species to the respective detection channel. It is useful to define an idealized system with perfect overlap of the observation volumes, $V_{eff,j} / V_{eff,x} = 1$, and negligible cross-talk. We indicate this with a small superscripted circle G_{kl}°. In this case, the fluorophores respond only to the channels they have been designed for, e.g. *(g)reen* $\rightarrow 1$ and *(r)ed* $\rightarrow 2$, and the *characteristic intensity* of a particle is proportional to the number of bound dyes, $\widetilde{F}_j^{(s)} = n_t F^{(t)}$. Normalizing with channel 1, Eq. (17) can be simplified to

$$RatioG_1^{\circ} = \frac{\sum_s c^{(s)} n_g^{(s)} n_r^{(s)}}{\sum_s c^{(s)} n_g^{(s)2}} \frac{c_0^{(g)}}{c_0^{(r)}} \qquad (18)$$

Here, $c_0^{(g)}$ and $c_0^{(r)}$ designate the total concentrations of green and red fluorophores, respectively. Furthermore, if we assume

a simple one-to-one interaction of single-labelled monomers (n_t=1),

$$RatioG_1^{\circ} = \frac{c^{(gr)}}{c_0^{(r)}} = \frac{c^{(gr)}}{c^{(gr)} + c^{(r)}} = \theta_2 \qquad (19)$$

directly reflects the fraction θ_2 of two-coloured particles. Note that $RatioG_1$ indicates the fraction θ_2 of the population labelled with the colour detected in channel 2, while channel 1 is used for normalization.

How can $RatioG_j^{\circ}$ be extracted, since focal geometry and cross-talk bias the experimental results? Eq. (19) suggests a straightforward experimental strategy: the system can be calibrated by measuring a standard assay, a series of mixtures between free and stably complexed dyes corresponding to the monomers and products of a binding reaction. This provides a direct relation between the measured $RatioG_j$ and a theoretical $RatioG_j^{\circ}$ solely reflecting the binding equilibrium of labelled monomers in solution (for details see [35]).

10. Instrumental Limitations for Measuring Interactions

The lower limit $RatioG_{j,min}$ for monitoring a binding reaction is defined by cross-talk. When merging two distinctly coloured populations of binding partners in solution, an initial baseline can directly be measured if the reaction is very slow or inducible by a binding relevant factor (e.g. reactions *c* and *d* in Table 1). Otherwise one has to measure the differently coloured populations separately in advance and can calculate the cross-talk-related offset using Eq. (17)

$$RatioG_{j,\min} = \frac{F_1^{(g)} F_2^{(g)} G_x^{(g)}(0) + F_1^{(r)} F_2^{(r)} G_x^{(r)}(0)}{F_j^{(g)2} G_j^{(g)}(0) + F_j^{(r)2} G_j^{(r)}(0)} \frac{F_j}{F_1 F_2} \qquad (20)$$

with $F_j = F_j^{(g)} + F_j^{(r)}$.

On the other hand, the upper limit $RatioG_{j,max}$ is affected by all aspects mentioned above: the geometry of the *detection functions*, background, cross-talk, and the stoichiometry of the complexed dyes. According to Eq. (5), the geometrical implications for $RatioG_j$ can be expressed analytically in terms of the displacement and the size of the respective observation volumes

$$\frac{\widetilde{G}_x(0)}{\widetilde{G}_j(0)} = \exp\left(-\frac{d_x^2 + d_y^2}{w_{0,eff}^2} - \frac{d_z^2}{z_{0,eff}^2} \right) \frac{V_{eff,j}}{V_{eff,x}} \qquad (21)$$

However, we suggest to determine the system with a standard solution of double-labelled particles carrying each of the fluorophores, in similar concentrations as used for monitoring the binding reaction. Such a calibration provides a value for $RatioG_{j,max}$ where all of the intensity and geometry-related influences are covered. Then, together with Eq. (20), the extent of a binding reaction can simply be defined as the fractional progress from min to max:

$$\theta_j = \frac{RatioG_j - RatioG_{j,\min}}{RatioG_{j,\max} - RatioG_{j,\min}} \qquad (22)$$

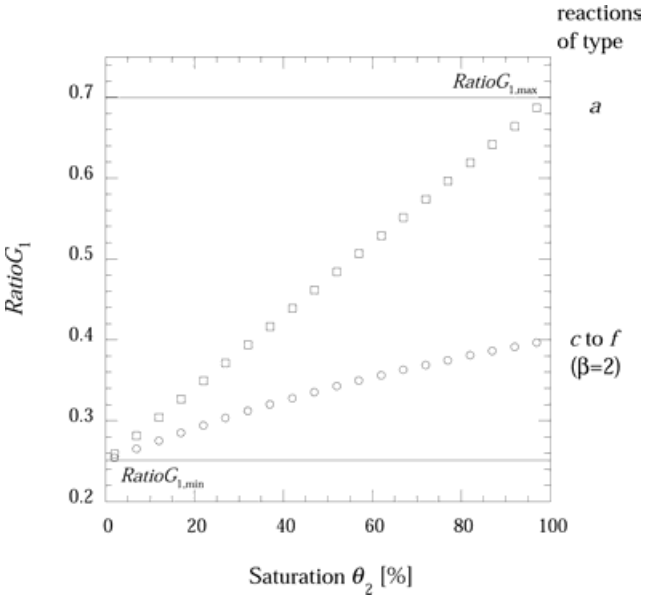

Fig. 5. *Ligand binding of uniformly labelled compounds at equilibrium. $RatioG_{1,max}$ was calculated according to a geometry as used for Fig. 3a, and $RatioG_{1,min}$ for 20% of cross-talk spilling into the red and 5% into the green channel. For heteronomous reactions of type a, $RatioG_1$ shows a linear dependence to the fraction of bound ligands $\theta_2 = c^{(gr)}/c_0^{(r)}$(squares). A homonomous dimerization as a special case of reactions of type c to f, with $\beta = 2$, is also shown (circles). Here, half of the monomers are green and the other half is red labelled. We parameterized the binding reaction with $\theta_2 = (c^{(gr)} + 2\, c^{(gg)})/c_0^{(r)}$ (to account for single-coloured dimers (for details see [35]) which reduce $RatioG_{1,max}$ to one third.*

11. Two-component interactions in equilibrium

Monitoring two-component interactions in a two-colour detection system allows two modes of experiments: either both of the participants carry different colours or just one compound can be labelled. Decisions in favour of one or the other system are usually based on the availability of labelled substrates. Some typical configurations are summarized in

interacting particles		labelled	
		one compound	both compounds
hetero-nomous	ligand binding	*c*: $A + \beta B^{(g)(r)} \rightleftharpoons AB_{\beta}^{(g)(gr)(r)}$	*a*: $A^{(g)} + \beta B^{(r)} \rightleftharpoons AB_{\beta}^{(gr)}$
	general stoichiometry	*d*: $\alpha A + \beta B^{(g)(r)} \rightleftharpoons A_{\alpha}B_{\beta}^{(g)(gr)(r)}$	*b*: $\alpha A^{(g)} + \beta B^{(r)} \rightleftharpoons A_{\alpha}B_{\beta}^{(gr)}$
homo-nomous	oligomerisation	*e*: $\beta B^{(g)(r)} \rightleftharpoons B_{\beta}^{(g)(gr)(r)}$	α, β, ν = stoichiometric integers A, B = compounds of the reaction $B^{(g)}$ = green labelled $B^{(r)}$ = red labelled $B^{(rg)}$ = two-coloured labelled $B^{(r)(g)}$ = mixture of green and red labelled particles
	multistep oligomerisation	*f*: $\beta B^{(g)(r)} \rightleftharpoons \beta/\nu B_{\nu}^{(g)(gr)(r)}$ $\cdots \rightleftharpoons B_{\beta}^{(g)(gr)(r)}$	

Tab. 1. *Reaction schemes. Two-component binding reactions are classified according to the possibilities for labelling the compounds. One or both types of interacting particles can be labelled. Thereby three basic reaction schemes arise which are further subdivided in order to distinguish increasing stoichiometric complexity; for details see section 11.*

Table 1 where three basic schemes arise: heteronomous binding monitored by both of the compounds (*a* and *b*), heteronomous binding monitored by one of the compounds (*c* and *d*), and oligomerization of a monomer (*e* and *f*). The following discussion wants to give a comprehensive rational to decide how $RatioG_j^{\circ}$ and binding are related for these different cases and which is the maximum value of $RatioG_j^{\circ}$ to be expected for a reaction driven to the side of fully formed products. For simplicity we assume here that all of the labelled monomers A and B of a binding assay show homogenous molecular brightness.

Labelling of both binding partners. Reactants A and B are labelled with green and red fluorophores, respectively. Applying Eq. (6) to Eq. (18) yields the most general expression for heteronomous reactions (type *b*) where the number of fluorophores can be replaced by the stoichiometric integers n_g, $n_r = \alpha, \beta$ such that

$$RatioG_1^{\circ} = \frac{\sum_{\alpha,\beta}\left[A_{\alpha}^{(g)}B_{\beta}^{(r)}\right]\alpha\beta}{\sum_{\alpha}\left[A_{\alpha}^{(g)}B_{\beta}^{(r)}\right]\alpha^2}\frac{\left[A_o^{(g)}\right]}{\left[B_0^{(r)}\right]}. \qquad (23)$$

Again we normalized with the green channel assigned to the reactants A which designate the receptors in the case of ligand binding (type *a)*. *Here, with* $\alpha=1$, Eq. (23) adopts a convenient form

$$RatioG_1^{\circ} = \frac{\sum_{\beta}\left[A^{(g)}B_b^{(r)}\right]\beta}{\left[B_b^{(r)}\right]}, \qquad (24)$$

where $RatioG_1^{\circ}$ reflects the fraction of bound ligand in agreement with Eq. (19) for $\beta=1$. Eq. (24) can be linked to the most general expression containing thermodynamic variables characterizing a multistep equilibrium, known as the *Adair-equation*

$$RatioG_1^{\circ}\frac{\left[B_0^{(r)}\right]}{\left[A_0^{(g)}\right]} = \frac{\sum_{\beta}\beta K^{(\beta)}\left[B^{(r)}\right]^{\beta}}{\sum_{\beta}K^{(\beta)}\left[B^{(r)}\right]^{\beta}}, \qquad (25)$$

where each subsequent step of the association is governed by its particular equilibrium $K^{(\beta)}$ constant . For reactions of this type, complete ligand binding leads to $RatioG_{1,\max}^{\circ}=1$, whereas in the general case the squared contribution of multiple receptors α in the denominator of Eq. (23) produces a slight reduction according to

$$RatioG_{1,\max}^{\circ} = \frac{3(\alpha+1)}{2(2\alpha+1)} \qquad (26)$$

Labelling one compound with two colours. Ligands B are labelled in green and red colour and lead to the formation of two- and one-coloured particles. Due to the symmetry of the system we do not need to specify the channel with which the cross-correlation is normalized. The distribution depends on the number of binding sites which is now a stoichiometric integer $n=\beta$ as well as on p_t the fraction of monomers which are labelled with a fluorophore of type *t*. The formalism to cover statistical association has been derived in section 6. We find

$$RatioG_j^{\circ} = \frac{\sum_\beta \left[B_\beta^{(g)(gr)(r)}\right]\beta(\beta-1)}{\sum_\beta \left[B_\beta^{(g)(gr)(r)}\right](\beta(\beta-1)+1/p_t)} \quad (27)$$

where the nascent complexes are sorted into β classes corresponding to their number of bound ligands. The sums have been executed for a binomial distribution of labelled monomers at the complex for each class. The expression is valid for all reactions of type *c* to *f* , since putative unlabelled compounds A give no signal. However, the reactions differ in the concentration dependence of $RatioG_1^{\circ}$ where an equilibrium is shifted to one or the other side. Eq. (27) may serve as a basis to distinguish the mechanisms by comparing simulated and measured data of a titration assay.

For both homonomous oligomerization reactions (type *e* and *f*), as well as for heteronomous reactions where only one compound is labelled (type *c* and *d*), the maximum value for $RatioG_j^{\circ}$ is a direct outcome of Eq. (19) and Eq. (20)

$$RatioG_{j,\max}^{\circ} = \frac{\beta-1}{\beta-1+1/p_t} \quad (28)$$

Fig. 5 illustrates some typical titrations curves of binding reactions in equilibrium. Whereas heteronomous receptor-ligand binding (type *a*) leads to a linear increase with saturation of the binding sites according to Eq. (24), the measurable range is dramatically reduced when only one compound can be labbelled. For a simple dimerization of equal amounts of green and red labelled components ($\beta = 2$ and $p_t = 1/2$), the maximium is reduced to one third compared to a heteronomous dimerization and even linearity of the dependency is lost.

Concluding Remarks

We have developed a general formalism for simultaneously describing auto- and cross-correlation amplitudes in FCS/FCCS for solutions of molecular species labelled with two spectrally distinguishable dyes. Extracting stoichiometric characteristics of a binding event on a molecular level requires first to account for technical implications such as imperfect overlap of the focal volumes, background signal, and cross-talk between the two channels. Given these parameters, our formalism allows the quantitative treatment of incomplete labelling and multiple binding or labelling sites. Although the instrumental resolution may not always allow to apply all of the quantitative dependencies mentioned, we think that the relationships derived here constitute a useful tool to extract binding equilibrium constants and stoichiometries, labelling efficiencies and other thermodynamic and molecular parameters from FCS/FCCS data.

It is striking that most quantitative binding studies by FCCS were done on protein/DNA or DNA/DNA systems with labeled DNA, and to our knowledge no quantitative characterization of pure protein-protein interactions has been reported. The reasons may be problems in preparation and purification of spectrally well defined derivatives, as well as in the quantitative treatment of more complex situations often encountered in molecular biology. To help in their interpretation is an aim of the current contribution.

Appendix

A. Analytical 3-D Correlation Function with Chromatic Displacement

We have seen in Eq. (4) that the correlation function of *N* uniform particles can be reduced to the correlation of a single one

$$G_{kl}(\tau) = \frac{1}{N}\frac{\langle f_k(\vec{r}(0))f_l(\vec{r}(\tau))\rangle}{\langle f_k\rangle\langle f_l\rangle}. \quad (A1)$$

The probability to find a particle at position $\vec{r}_1$ at time zero is d^3r_1/V . The probability to observe it at position after a given time τ due to Brownian motion can be expressed analytically by $P_D(\vec{r}_2|\vec{r}_1,\tau)d^3r_2$, the diffusion propagator, which is a solution of Fick's second law with the boundary condition $c(\vec{r},0) = \delta(\vec{r})$

$$P_D(\vec{r}_2|\vec{r}_1,\tau) = (4\pi D\tau)^{-3/2}\exp\left(-\frac{|\vec{r}_2-\vec{r}_1|^2}{4D\tau}\right). \quad (A2)$$

Its signal contribution at time zero in channel *k* is proportional to $\Psi_k(\vec{r}_1)$, thus $f_k(0)f_l(\tau) \propto \Psi_k(\vec{r}_1)\Psi_l(\vec{r}_2)$, and yields an analytical expression of Eq. (A1)

$$G_{kl}(t) = \frac{V}{N}\frac{\int_V\int_V d^3r_1 d^3r_2 \Psi_k(\vec{r}_1)P_D(\vec{r}_2|\vec{r}_1,\tau)\Psi_l(\vec{r}_2)}{\int_V d^3r_1\Psi_k(\vec{r}_1)\int_V d^3r_1\Psi_l(\vec{r}_1)} \quad (A3)$$

Integration is done by introducing $\Psi_j(\vec{r})$ as three dimensional Gaussian functions with $1/e^2$-radii z_0 parallel and w_0 perpendicular to the optical axis *z*

$$\Psi_j(\vec{r}) = \exp\left(-2\frac{(x-p_x)^2+(y-p_y)^2}{w_{0,j}^2} - 2\frac{(z-p_z)^2}{z_{0,j}^2}\right) \quad (A4)$$

and extending the limits to infinity. Here $\vec{p}$ is the displacement vector between the centres of the two foci.

B. Statistical Relations

The *i*-th moment of a trinomial distribution is determined by the *i*-th derivative of the dedicated generating function $(p_a + p_b + p_c)^2$.
First moment:

$$\frac{\partial}{\partial p_a}(p_a + p_b + p_c)^n = \frac{\partial}{\partial p_a}\sum_{n_a+n_b=0}^{n}\binom{n}{n_a}\binom{n-n_a}{n_b}p_a^{n_a}p_b^{n_b}p_c^{n-n_a-n_b}$$

$$\underbrace{n(p_a + p_b + p_c)^{n-1}}_{=1} = \sum_{n_a+n_b=0}^{n}\binom{n}{n_a}\binom{n-n_a}{n_b}n_a p_a^{n_a-1}p_b^{n_b}p_c^{n-n_a-n_b}$$

$$= np_a\sum_{n_a+n_b=0}^{n} n_a P(n_a, n_b) \qquad \text{(B1)}$$

Second moments in analogy:

$$n(n-1)p_a p_b = \sum_{m_a+m_b=0}^{m} n_a n_b P(n_a, n_b) \qquad \text{(B2)}$$

$$n(n-1)p_a^2 + np = \sum_{n_a+n_b=0}^{n} n_a^2 P(n_a, n_b) \qquad \text{(B3)}$$

Acknowledgements This work was funded by the Volkswagen foundation through the program “Physics, Chemistry and Biology with Single Molecules”. We thank Konstantin Klenin for helpful discussions.

References

[1] Langowski, J., Tewes, M., in Protein-DNA Interactions: A Practical Approach Travers, A., Buckle, M., Eds. (Oxford University Press, Oxford, 2000) pp. 95-111.
[2] Magde, D., Elson, E. L., Webb, W. W., Thermodynamic fluctuations in a reacting system - measurement by fluorescence correlations spectroscopy. Phys. Rev. Let. (1972) **29**, 705-708.
[3] Elson, E. L., Magde, D., Fluorescence correlation spectroscopy. I. Conceptual basis and theory. Biopolymers (1974) **13**, 1-27.
[4] Webb, W. W., Applications of fluorescence correlation spectroscopy. Q Rev Biophys (1976) **9**, 49-68.
[5] Qian, H., Elson, E. L., Analysis of Confocal Laser-Microscope Optics for 3-D Fluorescence Correlation Spectroscopy. Appl. Opt. (1991) **30**, 1185-1195.
[6] Rigler, R., Mets, Ü., Widengren, J., Kask, P., Fluorescence correlation spectroscopy with high count rate and low background: analysis of translational diffusion. Eur. Biophys. J. (1993) **22**, 169-175.
[7] Rigler, R., Widengren, J., Eds., Interactions and kinetics of single molecules as observed by fluorescence correlation spectroscopy (Springer Publishing Co., New York, 1993).
[8] Eigen, M., Rigler, R., Sorting single molecules: Application to diagnostics and evolutionary biotechnology. Proc. Natl Acad. Sci. USA (1994) **91**, 5740-5747.
[9] Kettling, U., Koltermann, A., Schwille, P., Eigen, M., Real-time enzyme kinetics monitored by dual-color fluorescence cross- correlation spectroscopy. Proc. Natl. Acad. Sci. USA (1998) **95**, 1416-1420.
[10] Koltermann, A., Kettling, U., Bieschke, J., Winkler, T., Eigen, M., Rapid assay processing by integration of dual-color fluorescence cross-correlation spectroscopy: high throughput screening for enzyme activity. Proc. Natl. Acad. Sci. USA (1998) **95**, 1421-1426.
[11] Langowski, J., Wachsmuth, M., Rippe, K., Tewes, M., in Energies et forces de l'interaction entre macromolécules biologiques: l'aspect quantitatif Frénoy, J.-P., Ed. (Publications CNRS, Paris, 2000), vol. **2**, pp. 65-77.
[12] Ricka, J., Binkert, T., Direct measurement of a distinct correlation function by fluorescence cross correlation. Phys. Rev. A. (1989) **39**, 2646-2652.
[13] Rigler, R., et al., Fluorescence cross-correlation: a new concept for polymerase chain reaction. J. Biotechnol. (1998) **63**, 97-109.
[14] Schwille, P., Meyer-Almes, F. J., Rigler, R., Dual-color fluorescence cross-correlation spectroscopy for multicomponent diffusional analysis in solution. Biophys. J. (1997) **72**, 1878-1886.
[15] Aragón, S. R., Pecora, R., Fluorescence correlation spectroscopy as a probe of molecular dynamics. J. of Chem. Phys. (1976) **64**, 1791-1803.
[16] Palmer, A. G., Thompson, N. L., Optical spatial intensity profiles for high order autocorrelation in fluorescence spectroscopy. Appl. Opt. (1989) **28**, 1214-1220.
[17] Sorscher, S. M., Klein, M. P., Profile of a focused collimated laser beam near the focal minimum characterized by fluorescence correlation spectroscopy. Rev. Sci. Instrum. (1980) **51**, 98-102.

[18] Widengren, J., Rigler, R., Fluorescence correlation spectroscopy as a tool to investigate chemical reactions in solutions and on cell surfaces. Cell Mol Biol (Noisy-le-grand) (1998) **44**, 857-79.
[19] Chen, Y., Müller, J. D., Berland, K. M., Gratton, E., Fluorescence Fluctuation Spectroscopy. Methods (1999) **19**, 234-252.
[20] Widengren, J., Mets, Ü., Rigler, R., Fluorescence Correlation Spectroscopy of Triplet States in Solution: A Theoretical and Experimental Study. J. Phys. Chem. (1995) **99**, 13368-13379.
[21] Haupts, U., Maiti, S., Schwille, P., Webb, W. W., Dynamics of fluorescence fluctuations in green fluorescent protein observed by fluorescence correlation spectroscopy. Proc. Natl Acad. Sci. USA (1998) **95**, 13573-13578.
[22] Schwille, P., Kummer, S., Heikal, A. A., Moerner, W. E., Webb, W. W., Fluorescence correlation spectroscopy reveals fast optical excitation- driven intramolecular dynamics of yellow fluorescent proteins. Proc. Natl. Acad. Sci. USA (2000) **97**, 151-156.
[23] Palmer, A. G. d., Thompson, N. L., Molecular aggregation characterized by high order autocorrelation in fluorescence correlation spectroscopy. Biophys J (1987) **52**, 257-70.
[24] Palmer, A. G., Thompson, N. L., High-order fluorescence analysis of model protein clusters. Proc. Natl. Acad. Sci. USA (1989) **86**, 6148-6152.
[25] Qian, H., Elson, E. L., On the Analysis of High-Order Moments of Fluorescence Fluctuations. Biophys. J. (1990) **57**, 375-380.
[26] Qian, H., Elson, E. L., Distribution of molecular aggregation by analysis of fluctuation moments. Proc. Natl. Acad. Sci. USA (1990) **87**, 5479-5483.
[27] Chen, Y., Muller, J. D., So, P. T., Gratton, E., The photon counting histogram in fluorescence fluctuation spectroscopy. Biophys J (1999) **77**, 553-567.
[28] Kask, P., Palo, K., Ullmann, D., Gall, K., Fluorescence-intensity distribution analysis and its application in biomolecular detection technology. Proc Natl Acad Sci U S A (1999) **96**, 13756-13761.
[29] Pack, C. G., et al., Analysis of interaction between chaperonin GroEL and its substrate using fluorescence correlation spectroscopy. Cytometry (1999) **36**, 247-53.
[30] Post, K., et al., Rapid acquisition of beta-sheet structure in the prion protein prior to multimer formation. Biol Chem (1998) **379**, 1307-1317.
[31] Sevenich, F. W., Langowski, J., Weiss, V., Rippe, K., DNA binding and oligomerization of NtrC studied by fluorescence anisotropy and fluorescence correlation spectroscopy. Nucleic Acids Res. (1998) **26**, 1373-1381.
[32] Tjernberg, L. O., et al., Amyloid beta-peptide polymerization studied using fluorescence correlation spectroscopy. Chem Biol (1999) **6**, 53-62.
[33] Van Craenenbroeck, E., Engelborghs, Y., Quantitative characterization of the binding of fluorescently labeled colchicine to tubulin in vitro using fluorescence correlation spectroscopy. Biochemistry (1999) **38**, 5082-8.
[34] Foldes-Papp, Z., Rigler, R., Quantitative two-color fluorescence cross-correlation spectroscopy in the analysis of polymerase chain reaction. Biol Chem (2001) **382**, 473-8.
[35] Rippe, K., Simultaneous binding of two DNA duplexes to the NtrC-enhancer complex studied by two-color fluorescence cross-correlation spectroscopy. Biochemistry (2000) **39**, 2131-2139.
[36] Tewes, M., Aufbau eines Experiments zur Fluoreszenzkreuzkorrelationsspektroskopie, Erweiterung der theoretischen Grundlagen und biologische Anwendungen. PhD thesis, University of Heidelberg, 1998.
[37] Magde, D., Elson, E. L., Webb, W. W., Fluorescence correlation spectroscopy. II. An experimental realization. Biopolymers (1974) **13**, 29-61.
[38] Edelmann, P., Esa, A., Hausmann, M., Cremer, C., Confocal laser-scanning fluorescence microscopy: In situ determination of the confocal point-spread function and the chromatic shifts in intact cell nuclei. Optik (1999) **110**, 194-198.
[39] Esa, A., et al., Three-dimensional spectral precision distance microscopy of chromatin nanostructures after triple-colour DNA labelling: a study of the BCR region on chromosome 22 and the Philadelphia chromosome. J Microsc (2000) **199**, 96-105.
[40] Lamb, D. C., Schenk, A., Rocker, C., Scalfi-Happ, C., Nienhaus, G. U., Sensitivity enhancement in fluorescence correlation spectroscopy of multiple species using time-gated detection. Biophys J (2000) **79**, 1129-38.
[41] Meseth, U., Wohland, T., Rigler, R., Vogel, H., Resolution of fluorescence correlation measurements. Biophys. J. (1999) **76**, 1619-1631.
[42] Thompson, N. L., in Topics in Fluorescence Spectroskopy Lakowicz, J. R., Ed. (Plenum Press, New York, 1991), vol. 1, pp. 337-378.
[43] Koppel, D., Statistical accuracy in fluorescence correlation spectroscopy. Phys. Rev. A (1974) **10**, 1938-1945.